PHYSICS

Chaos-assisted tunneling resonances in a synthetic Floquet superlattice

M. Arnal[1], G. Chatelain[1], M. Martinez[2], N. Dupont[1], O. Giraud[3], D. Ullmo[3], B. Georgeot[2], G. Lemarié[2], J. Billy[1], D. Guéry-Odelin[1]*

The field of quantum simulation, which aims at using a tunable quantum system to simulate another, has been developing fast in the past years as an alternative to the all-purpose quantum computer. So far, most efforts in this domain have been directed to either fully regular or fully chaotic systems. Here, we focus on the intermediate regime, where regular orbits are surrounded by a large sea of chaotic trajectories. We observe a quantum chaos transport mechanism, called chaos-assisted tunneling, that translates in sharp resonances of the tunneling rate and provides previously unexplored possibilities for quantum simulation. More specifically, using Bose-Einstein condensates in a driven optical lattice, we experimentally demonstrate and characterize these resonances. Our work paves the way for quantum simulations with long-range transport and quantum control through complexity.

INTRODUCTION

The fast-growing field of quantum simulations benefits from a wide variety of experimental techniques (*1*–*8*). Among them, the use of temporal driving has attracted a huge interest recently as it was shown that certain fast drivings can create new topological effects (*9*–*14*), while a strong driving leads to, e.g., Anderson localization physics (*15*–*20*). In the intermediate regime, characterized by a rich classical phase space where stable trajectories form islands surrounded by a large sea of unstable chaotic orbits, another type of quantum transport, called chaos-assisted tunneling (*21*–*27*), can take place between the regular islands. Such a system mimics an effective superlattice for the quantum states localized in the regular islands, with new controllable tunneling properties. Besides the standard textbook tunneling through a potential barrier, chaos-assisted tunneling corresponds to a much richer tunneling process, where the coupling between quantum states located in neighboring regular islands is mediated by other states spread over the chaotic sea.

In classical dynamical systems, a major progress of the last century has been the understanding that many systems display various degrees of chaos (*28*). Strongly chaotic systems are characterized by exponential sensitivity to initial conditions and ergodicity of a typical trajectory in phase space. These properties can be seen in very simple systems: in astronomy (*29*), in chemistry (*30*), in biology (*31*, *32*), and in ecology (*33*, *34*). Most systems exhibit a mixed phase space in which chaotic and regular zones coexist. While chaotic behavior is difficult to predict, the instability that emerges in such systems makes them very versatile as a small perturbation can induce a completely different evolution. Even more, this instability can be harnessed to tune the system to a desired final state at a minimal cost, a process dubbed "control of chaos" (*35*–*37*).

In the field of quantum simulation, the emphasis has been put on the use of regular systems, which are a priori easier to control. Here, we show that using chaotic dynamics in a cold atom setting actually opens possibilities for quantum simulations, which are difficult to reach by other means. To do so, we use periodically driven systems, which are a paradigm for the study of quantum chaos, as the strength of the modulation can be used to control the level of chaos (*28*, *38*, *39*). More precisely, we consider ultracold atoms in a one-dimensional (1D) optical lattice, whose depth is periodically modulated in time (*40*, *41*). For a moderately strong modulation, we generate a mixed phase space with regular islands surrounded by a chaotic sea (see Fig. 1). The quantum mechanics of such a system leads to quantum states, which are either localized on the regular islands or spread over the chaotic sea (*42*, *43*). This picture emerges in the semiclassical limit, where the quantum scale represented by the Planck constant $\hbar$ is smaller than the typical area of the classical structures. Then, the regular islands form an effective lattice, whose properties can be modified by varying the temporal modulation. More precisely, we demonstrate that, in such a driven lattice, the position and the number of regular islands as well as the size of the surrounding chaotic sea can be finely tuned.

Another key phenomenon of purely quantum origin lies in the modification of the tunnel effect in such a mixed system. Quantum states can cross the classically forbidden dynamical barriers through a process similar to the standard tunneling called dynamical tunneling (*44*, *45*). This dynamical tunneling can be strongly affected by the presence of the chaotic states (*21*, *46*–*63*), which results in large variations of the tunneling rate over a short range of parameter, leading to so-called chaos-assisted tunneling resonances (*21*, *46*). This effect has been experimentally observed with great precision for electromagnetic waves (*24*–*27*, *64*, *65*). For matter waves, dynamical and chaos-assisted tunneling between regular islands were achieved in the pioneering experiments (*22*, *23*, *66*). However, experimental limitations had made it impossible to clearly observe the sharp resonances, which are the hallmark of chaos-assisted tunneling (*40*, *41*, *67*–*70*). In this study, we show that in our ultracold atoms system, we are able to experimentally produce an effective tunable superlattice and observe the chaos-assisted tunneling resonances between spatially separated stable islands, allowing us to control tunneling of cold atoms from full suppression to strong enhancement in a small range of parameters.

[1]Laboratoire Collisions Agrégats Réactivité, IRSAMC, Université de Toulouse, CNRS, UPS, France. [2]Laboratoire de Physique Théorique, IRSAMC, Université de Toulouse, CNRS, UPS, France. [3]Université Paris-Saclay, CNRS, LPTMS, 91405 Orsay, France.
*Corresponding author. Email: dgo@irsamc.ups-tlse.fr

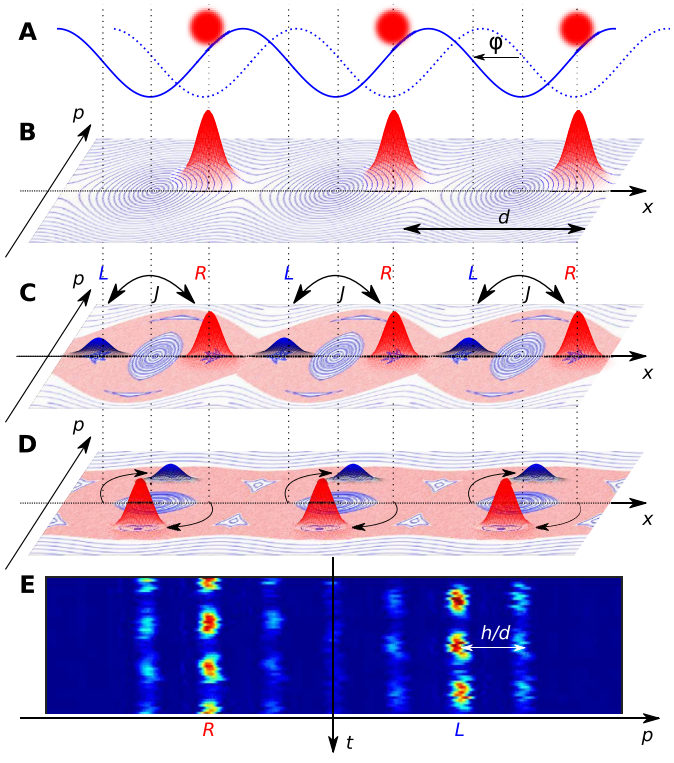

Fig. 1. Sketch of the experimental procedure. (**A**) By an abrupt phase shift φ of the lattice, the atomic clouds, initially at the bottom of the static lattice wells (blue dotted line), are suddenly placed on the slope of the shifted lattice wells (blue solid line). In the phase space (*x*,*p*) representation shown in (**B**), it corresponds to a displacement along the *x* axis. (**C**) The amplitude modulation of the lattice depth generates a mixed phase space with regular islands (blue closed orbits) surrounded by a chaotic sea (red zone). With the appropriate phase shift before the modulation, the wave packet can be placed on a lateral regular island (e.g., the right one). Then, the wave packet tunnels back and forth between the two stable symmetric lateral islands (tunneling rate *J*), leading to two wave packets *R* and *L*. (**D**) The observation of the tunneling requires a phase space rotation (black arrows), which transfers to momentum space the information encoded in position space: The population on the right (resp. left) island gains a negative (resp. positive) momentum. (**E**) Stack of integrated experimental images taken every two modulation periods. The images reflect the momentum distribution after a 25-ms time of flight, its periodicity *h*/*d* is directly related to the lattice periodicity. Classically, atoms are expected to stay on the same side (initially in the right island). The first three experimental tunneling oscillations are shown.

RESULTS

Experimental setup

Our experimental study is performed on a rubidium-87 Bose-Einstein condensate (BEC) machine, based on a hybrid trap (*71*). We superimpose to the horizontal optical dipole beam (*x* axis) of the trap a 1D optical lattice obtained from the interference of two counter-propagating laser beams. We engineer the phase and amplitude of the lattice via three acousto-optic modulators (*72*): One is dedicated to the control of the lattice laser intensity, and the others, driven by phase-locked synthesizers, control the relative phase, φ, between the two lattice beams. Introducing the dimensionless variables $p = 2\pi P/(m\omega d)$, $x = 2\pi X/d$, where m is the atomic mass, d = 532 nm is the lattice spacing, and X and P are the position and momentum along the standing wave and normalizing the time t to the modulation angular frequency ω, the Hamiltonian that governs the dynamics reads (*40*, *41*)

$$H = \frac{p^2}{2} - \gamma(1 + \varepsilon\cos(t))\cos(x + \varphi(t)) \quad (1)$$

Here, ε is the amplitude of the lattice depth modulation and $\gamma = s(\omega_L/\omega)^2$, with the dimensionless depth s of the lattice measured in units of the lattice characteristic energy $E_L = h^2/(2md^2) = \hbar\omega_L$. In practice, the dimensionless depth s is precisely calibrated by monitoring the center-of-mass motion of the wave packets inside the lattice sites (*73*). The quantum dynamics in that system is controlled by an effective tunable Planck constant $\hbar_{\text{eff}} = 2\omega_L/\omega$, which gives the typical area occupied by a minimal wave packet in a dimensionless phase space (*28*). Here, $\hbar_{\text{eff}}$ is thus an experimental parameter that effectively controls the quantum scale in the simulated system. It can be modified independently of γ and ε and thus for a fixed classical phase space.

To experimentally implement this Hamiltonian, we first load the BEC in a static lattice by a smooth increase of the lattice intensity (*72*). We then apply the protocol (*41*) described in Fig. 1: The lattice is suddenly shifted at the desired position by an abrupt change of the phase φ, and its amplitude is subsequently modulated for an even number of modulation periods $n \times 2T$ (see below). To perform measurements on our system, we continue the modulation for an extra $T/2$ duration. This amounts to performing a π/2 rotation in phase space to transfer in momentum space the information encoded in position space (see Supplementary Text) (*41*, *71*). After a 25-ms time of flight, the interferences between the matter waves originating from the different cells of the optical lattice create a diffraction pattern (see Figs. 1E and 2, A and B), from which the local population in the islands can be reconstructed (see Materials and Methods).

Classical dynamics and bifurcation

The classical dynamics generated by the periodic Hamiltonian of Eq. 1 is made apparent by a stroboscopic phase space map, plotting the (x, p) values at every modulation period. Typical (x, p) spaces (phase spaces) are displayed in Fig. 1 and show mixed dynamics with chaotic (red) and regular (blue) orbits. These orbits organize themselves in specific structures: regular islands made of stable periodic orbits, surrounded by a chaotic sea bounded in momentum by large-p regular zones (whispering galleries). Qualitatively, the value of the modulation amplitude ε mostly affects the size of the chaotic sea. By increasing γ in the range [0.18,0.36] at fixed ε = 0.268, the initial central stable island splits into two, and even three, stable islands (see Fig. 2C) (*41*, *74*). This process is a Hopf-type bifurcation well known in dynamical systems (see Supplementary Text) (*75*). Beyond the first bifurcation, classical trajectories starting from one island reach the symmetric island at each period. As a result, classical atoms remain in the same island when observed every two periods. To highlight the quantum tunneling dynamics, we therefore probe the system after an even number of modulation periods.

To characterize such dynamical bifurcations in phase space, we apply the modulation for a short even number of periods (between 4 and 10) to a packet of atoms initially placed at different positions along the x axis. The dynamics at short time is essentially classical, as quantum interferences do not manifest themselves yet. When the initial wave packet is placed into a stable island, we observe a diffraction pattern after time of flight with only a few orders populated

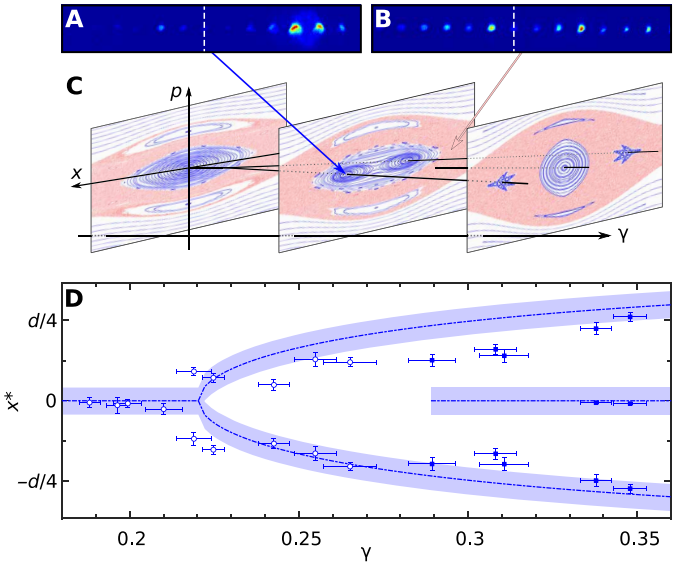

Fig. 2. Observation of the bifurcation. (**A** and **B**) Typical images obtained after time of flight, when the wave packet lay initially in a regular island or in the chaotic sea, respectively. In case (A), the momentum distribution remains narrow, while the wave function spreads over many orders in case (B). On both images, the white dashed line indicates the zero-momentum component. (**C**) Evolution of the stroboscopic phase space for increasing values of the dimensionless depth γ and fixed ε = 0.268, showing the splitting of the initial central regular island into two and then into three islands. Phase portraits were realized with 10,000 iterations of 107 initial positions equally spaced on the *x* and *p* axes. (**D**) Evolution of the position of the center of the regular islands, as a function of γ: experimental results obtained for $\hbar_{\mathrm{eff}} = 0.203$ (empty marks) and $\hbar_{\mathrm{eff}} = 0.232$ (filled marks). The analytical prediction is indicated as a dot-dashed line. The shaded area reveals the limited resolution governed by $\hbar_{\mathrm{eff}}$.

(see Fig. 2A). This is to be contrasted with the pattern observed when atoms are placed into the chaotic sea, where many orders are populated (see Fig. 2B). The measurement of the standard deviation (SD) of the momentum distribution therefore provides information on the initial position (in a chaotic or a regular region) in phase space along the *x* direction (see Materials and Methods). More specifically, the initial wave packet position x_0 that leads to a minimal momentum SD corresponds to the center of the regular islands. The island positions measured experimentally are in global agreement with the analytical prediction (see Fig. 2D) (*41*). The major discrepancies appear close to the critical values γ = 0.22 and γ = 0.29, where bifurcations actually take place. Close to those bifurcation points, a relatively small distance separates the islands, and we probe the classical bifurcation with a finite resolution dictated by the value of $\hbar_{\mathrm{eff}}$ ranging from 0.2 to 0.23 for our experimental parameters. We attribute the slight offset of the experimental results toward negative values to a mismatch between the phase shift we program and the one that is experienced by the atoms. Our measurements show that it is of the order of 2% of the lattice spacing *d*.

This splitting of the central island actually generates a synthetic stroboscopic superlattice with two characteristic lengths: the spacing *d* = 532 nm of the original lattice, and the distance between the stable islands, tunable from 50 to 250 nm, in a given cell. The corresponding stroboscopic quantum dynamics is described in terms of eigenstates $|\psi_n\rangle$ of the Floquet operator U_{F} (the evolution operator over two periods of modulation). Each Floquet eigenstate is associated with a quasi-energy ε_n such that $U_{\mathrm{F}}|\psi_n\rangle = \exp\left(-i\frac{\varepsilon_n 2T}{\hbar_{\mathrm{eff}}}\right)|\psi_n\rangle$. As a consequence, the stroboscopic dynamics can be linked to an effective time-independent Hamiltonian with eigenstates $|\psi_n\rangle$ and associated energies ε_n.

Chaos-assisted tunneling

To characterize chaos-assisted tunneling, we choose the regime for which two *x*-symmetric regular islands appear inside the chaotic sea. While a classical trajectory starting from a regular island will remain on the same island when observed every two periods (see above), a quantum wave packet initially located on a stable island will oscillate between the two symmetric islands due to the tunneling effect.

The standard tunneling effect, as described in textbooks for regular systems, involves only a doublet of quasi-degenerate symmetric and antisymmetric states localized on two symmetric islands. The tunneling period is proportional to the inverse of the splitting between these two states. In this case of regular dynamical tunneling (in the absence of a chaotic sea), the splitting is a smooth function of the parameters of the system, being an exponential of a classical action divided by $\hbar$.

Figure 3 illustrates the mechanism of chaos-assisted tunneling. In the presence of the chaotic sea, the tunnel effect between the islands is generically mediated by an additional chaotic state that interacts with one of the regular eigenstates having the same symmetry (see Fig. 3, A and C to F) (*21*). This interaction causes an avoided crossing between the regular and the chaotic levels, which, in turn, can greatly modify the splitting between the two regular levels (see Fig. 3, A and B). As the number of chaotic states is large in the semiclassical limit, these crossings are numerous and translate into large and erratic resonances of the tunneling rate when varying a parameter.

In Fig. 4, the experimentally measured oscillation frequencies are plotted as a function of $1/\hbar_{\mathrm{eff}}$, keeping all other parameters fixed, in two different phase space configurations. In the first configuration (regular dynamical tunneling), there is no chaotic sea between the two islands, and we experimentally observe a smooth exponential decay of the frequency as a function of $1/\hbar_{\mathrm{eff}}$. The two islands are actually "protected" by the regular tori within which they lie, which markedly reduces the possibility for the dynamics to be contaminated with a state from the chaotic sea. In the second configuration, the two islands are separated by a chaotic sea, and we observe large nonmonotonic variations of the tunneling frequency. The experimental data agree very well with numerical simulations, with no fitting parameter. At the resonance, the tunneling oscillations exhibit a beating with two frequencies (see Fig. 4E). This phenomenon is a clear signature of the three-level mechanism of chaos-assisted tunneling. The apparent discrepancy observed at resonance with the simplest theory built from the translationally invariant case originates from the finite spatial extension of the atomic wave packet in the optical lattice. Realistic numerical simulations including such effects agree very well with the experimental data (see Fig. 4, D to F).

DISCUSSION

We have observed similar chaos-assisted resonances at different parameter values (see Supplementary Text). The choice of the stable islands symmetric in position was motivated by their relatively large

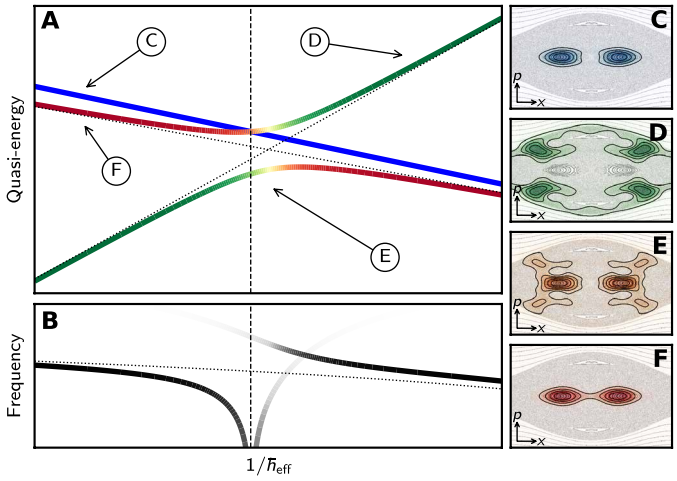

Fig. 3. Sketch of a chaos-assisted tunneling (CAT) resonance resonance. (**A**) Quasi-energy spectrum of a regular doublet (red and blue) and a chaotic (green) state. An avoided crossing occurs between the chaotic (green) state and the regular state (red) part of the doublet having the same symmetry. As $\hbar_{\mathrm{eff}}$ is varied, these two states mix and repel. (**B**) The resulting tunneling oscillation frequencies (proportional to differences in quasi-energies) exhibit two contributions and strong variations. (**C** to **F**) Phase space representations of quantum states involved in the crossing [Husimi function; see (*84*)]. Regular, antisymmetric (C) and symmetric (F) states are localized near integrable orbits; the chaotic states (D) lie in the chaotic sea, while the mixed one (E) overlaps with both structures.

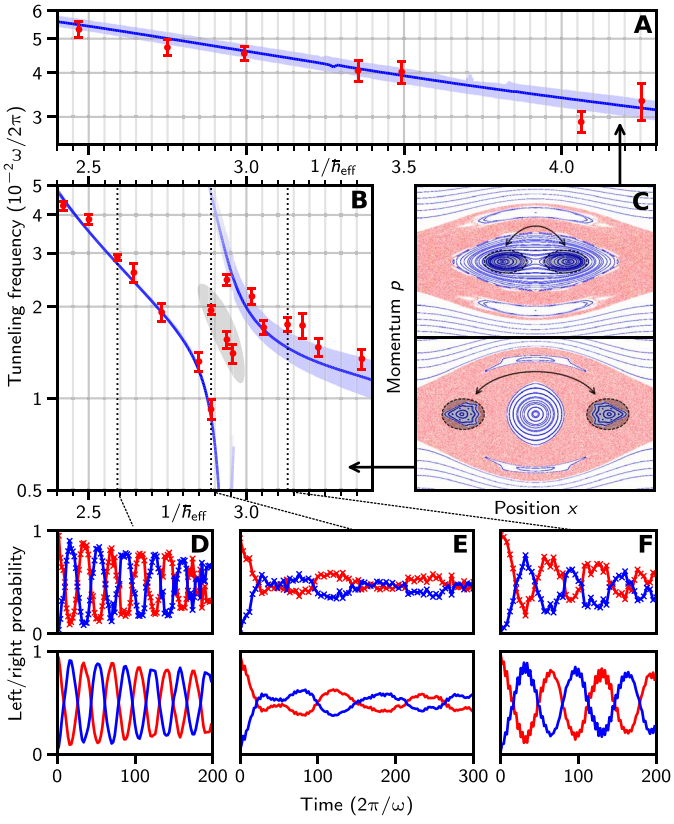

Fig. 4. Experimental observation of a CAT resonance and comparison with regular dynamical tunneling. (**A** and **B**) Experimentally measured tunneling frequencies (red dots) as a function of $\hbar_{\mathrm{eff}}^{-1}$ compared with numerical simulation in the case where all lattice cells are equally populated (blue lines) for the parameters (A) $\varepsilon = 0.14$, $\gamma = 0.249 \pm 0.002$ and (B) $\varepsilon = 0.24$, $\gamma = 0.375 \pm 0.005$. Tunneling frequencies are extracted through Fourier transform of the experimental or numerical oscillations (see Materials and Methods). Blue shaded area corresponds to the experimental uncertainty on γ, with a shade intensity giving the height of the Fourier peak. The gray shaded area of (B) reveals the zone in which a good agreement with experiments requires realistic simulations that take into account the initial finite size of the BEC (see Materials and Methods). The corresponding stroboscopic classical phase spaces are plotted in (**C**). (**D** to **F**) Population in each island and for different values of $\hbar_{\mathrm{eff}}^{-1}$ [corresponding to the dotted lines in (B)] as a function of time (blue, left island; red, right island); top: experimental data, bottom: realistic simulations with 13 cells initially equally populated. The first three oscillations of (D) are represented in Fig. 1E.

size, a characteristic that facilitates the efficient loading of the BEC, and the robustness of the expected tunnel oscillation with respect to the quasi-momentum width (*41*). The period-2 nature of the resonance [also suggested in (*76*)] leads to a situation where the symmetry is a classical property independent of quasi-momentum. The observation of a large number of oscillations was also made possible thanks to a careful experimental protocol: (i) The optical confinement of the BEC is made with far-off resonance lasers to avoid the deleterious effect of spontaneous emission, (ii) gravity is compensated for by a horizontal guide superimposed to the lattice, (iii) an optical lattice with a depth tunable over a large range, and (iv) the use of BECs to minimize the size in phase space and with a low number of atoms ($\sim 10^4$). The very same experiment performed with a larger number of atoms ($>10^5$) yields a strong damping of the tunneling oscillations (see Supplementary Text). We attribute the damping of these oscillations to interaction effects.

We have shown that the intermediate regime of temporal driving that we have studied allows to design tunable effective superlattices through phase space engineering. Moreover, we have demonstrated that the presence of chaos leads to chaos-assisted tunneling resonances between sites of the superlattice, which we have observed experimentally in a quantum system.

This new type of control through complexity via temporal driving is fairly generic. Interestingly enough, in the context of cold atoms, the tunneling resonances that we have demonstrated are species independent, in contrast to the well-known Feshbach resonances for interactions (*77*).

Chaos-assisted tunneling should allow to probe models with a new kind of long-range hoppings for quantum simulation not mediated by interactions (*78*–*80*). Chaos-assisted tunneling implies mediation by a state delocalized in the chaotic sea, which surrounds all the lattice sites. As a result, it leads to long-range hoppings across the system. These long-range models have been extensively studied theoretically in condensed matter and exhibit a rich phenomenology such as multifractality [power-law random banded matrices (*81*)], spin-glass physics (*82*), high-T_c (critical temperature) superconductivity (*83*), etc. Our protocol offers a strategy to emulate such models with cold atoms.

MATERIALS AND METHODS

Reconstruction of the populations in the regular islands

Because of subwavelength spacing between the regular islands, we cannot measure in situ by optical means the atomic populations in each island. To circumvent this limitation, we use two experimental tricks: (i) We perform a $\pi/2$ phase space rotation: By letting the system evolve for an additional $T/2$ time in the modulated lattice, the

atomic wave packet initially on the right (resp. left) island acquires a negative (resp. positive) momentum (see Supplementary Text); (ii) we subsequently switch off all trapping potentials and perform a 25-ms time of flight before taking an absorption image.

The corresponding patterns (Fig. 1E and fig. S1, A to D) consist in regularly spaced interference peaks centered about discrete momenta $p_j = jh/d$, with j an integer and d the lattice spacing. We identify the zero-momentum peak position by a preliminary experiment performed on a static lattice. We then label each peak with its corresponding discrete momentum value. The population initially in the right (resp. left) island is then determined from the integration of the peaks with negative (resp. positive) momenta after the time of flight. Performing the experiment for different times in the modulated lattice (an even number of modulation periods $n \times 2T$), we infer the time evolution of the populations (see fig. S1I).

Bifurcation

For a given phase space (see fig. S2, A to C), we can probe experimentally the number and position(s) of the regular island(s) along the x axis. For this purpose, we load the lattice adiabatically and then shift suddenly the lattice by a distance Δx before modulating the lattice amplitude for a few modulation periods (an even number of periods between 4 and 10). This choice of modulation time results from a trade-off: The tunneling is still marginal, while the spreading of the wave packet when placed in the chaotic zone is clearly visible. The analysis is performed after a 25-ms time-of-flight absorption image, which reveals the momentum distribution. The dispersion in momentum is extracted from the integrated profile of the experimental images (see e.g., fig. S2, E to H). Using a multi-Gaussian fit of this momentum dispersion plotted as a function of the initial offset Δx (see fig. S2, D to F), we extract the position(s) for which the momentum dispersion is minimal and therefore infer the position(s) of the center(s) of the regular island(s).

Oscillation frequency extraction

To extract experimental oscillation frequencies (see Fig. 4 and figs. S4C and S5C), we compute the Fourier spectra of the time evolution of the left and right populations. We extract from their average a main peak and keep the secondary peaks only when their weight is at least 1/3 of the main one, a choice that captures efficiently the main characteristics of the oscillations. Each frequency is determined from a three-point average around the corresponding maximum. The error on the frequency determination is assumed to follow a triangular law around the maxima with an uncertainty of $\pm f_0/(2\sqrt{6})$, where f_0 is the sampling rate.

Numerical simulations

The numerical simulations compute the evolution of an interaction-free wave function in the time-dependent potential using the split-step method. For Fig. 4 (A and B) and figs. S4C and S5C, the dynamics is simulated on a single cell of size equal to the lattice spacing.

The mixed classical phase space exhibits two stable islands symmetric in position. The initial state is a Gaussian wave packet placed at the center of one of the islands with the following relations between the quadratic sizes in position and momentum $\Delta x = 2\Delta p$ to maximize the overlap with the classical lateral island. The observable probed every two periods is the modulus squared of the overlap either with the initial state or its symmetrical partner centered on the other island. The oscillation frequencies are obtained from the Fourier transform performed over 10,000 periods. In the more realistic simulations of Fig. 4 (D to F), we consider a system made of 151 cells, and we initially populate the same island on 13 successive cells.

The analysis in terms of Floquet eigenstates, relevant for Fig. 3, is inferred from the evolution operator (Floquet operator) over two periods (see Supplementary Text). Quasi-energies are directly extracted from the phase of the eigenvalues.

SUPPLEMENTARY MATERIALS

Supplementary material for this article is available at http://advances.sciencemag.org/cgi/content/full/6/38/eabc4886/DC1

REFERENCES AND NOTES

1. V. M. Kendon, K. Nemoto, W. J. Munro, Quantum analogue computing. *Phil. Trans. R. Soc. A* **368**, 3609–3620 (2010).
2. J. I. Cirac, P. Zoller, Goals and opportunities in quantum simulation. *Nat. Phys.* **8**, 264–266 (2012).
3. P. Hauke, F. M. Cucchietti, L. Tagliacozzo, I. Deutsch, M. Lewenstein, Can one trust quantum simulators? *Rep. Prog. Phys.* **75**, 082401 (2012).
4. T. Schaetz, C. R. Monroe, T. Esslinger, Focus on quantum simulation. *New J. Phys.* **15**, 085009 (2013).
5. I. M. Georgescu, S. Ashhab, F. Nori, Quantum simulation. *Rev. Mod. Phys.* **86**, 153–185 (2014).
6. C. Gross, I. Bloch, Quantum simulations with ultracold atoms in optical lattices. *Science* **357**, 995–1001 (2017).
7. I. Bloch, Quantum simulations come of age. *Nat. Phys.* **14**, 1159–1161 (2018).
8. M. Bellec, U. Kuhl, G. Montambaux, F. Mortessagne, Topological transition of dirac points in a microwave experiment. *Phys. Rev. Lett.* **110**, 033902 (2013).
9. N. H. Lindner, G. Refael, V. Galitski, Floquet topological insulator in semiconductor quantum wells. *Nat. Phys.* **7**, 490–495 (2011).
10. I.-D. Potirniche, A. C. Potter, M. Schleier-Smith, A. Vishwanath, N. Y. Yao, Floquet symmetry-protected topological phases in cold-atom systems. *Phys. Rev. Lett.* **119**, 123601 (2017).
11. M. C. Rechtsman, J. M. Zeuner, Y. Plotnik, Y. Lumer, D. Podolsky, F. Dreisow, S. Nolte, M. Segev, A. Szameit, Photonic floquet topological insulators. *Nature* **496**, 196–200 (2013).
12. N. R. Cooper, J. Dalibard, I. B. Spielman, Topological bands for ultracold atoms. *Rev. Mod. Phys.* **91**, 015005 (2019).
13. N. Goldman, J. Dalibard, Periodically driven quantum systems: Effective hamiltonians and engineered gauge fields. *Phys. Rev. X* **4**, 031027 (2014).
14. A. Eckardt, *Colloquium*: Atomic quantum gases in periodically driven optical lattices. *Rev. Mod. Phys.* **89**, 011004 (2017).
15. G. Casati, B. V. Chirikov, J. Ford, F. M. Izrailev, *Stochastic Behavior of a Quantum Pendulum Under Periodic Perturbation* (Springer-Verlag, 1979), vol. 93, pp. 334–352.
16. S. Fishman, D. R. Grempel, R. E. Prange, Chaos, quantum recurrences, and anderson localization. *Phys. Rev. Lett.* **49**, 509–512 (1982).
17. R. Graham, M. Schlautmann, D. L. Shepelyansky, Dynamical localization in Josephson junctions. *Phys. Rev. Lett.* **67**, 255–258 (1991).
18. F. L. Moore, J. C. Robinson, C. F. Bharucha, B. Sundaram, M. G. Raizen, Atom optics realization of the quantum δ-kicked rotor. *Phys. Rev. Lett.* **75**, 4598–4601 (1995).
19. G. Casati, I. Guarneri, D. L. Shepelyansky, Anderson transition in a one-dimensional system with three incommensurate frequencies. *Phys. Rev. Lett.* **62**, 345–348 (1989).
20. J. Chabé, G. Lemarié, B. Grémaud, D. Delande, P. Szriftgiser, J. C. Garreau, Experimental observation of the anderson metal-insulator transition with atomic matter waves. *Phys. Rev. Lett.* **101**, 255702 (2008).
21. S. Tomsovic, D. Ullmo, Chaos-assisted tunneling. *Phys. Rev. E* **50**, 145–162 (1994).
22. D. A. Steck, W. H. Oskay, M. G. Raizen, Observation of chaos-assisted tunneling between islands of stability. *Science* **293**, 274–278 (2001).
23. D. A. Steck, W. H. Oskay, M. G. Raizen, Fluctuations and decoherence in chaos-assisted tunneling. *Phys. Rev. Lett.* **88**, 120406 (2002).
24. C. Dembowski, H.-D. Gräf, A. Heine, R. Hofferbert, H. Rehfeld, A. Richter, First experimental evidence for chaos-assisted tunneling in a microwave annular billiard. *Phys. Rev. Lett.* **84**, 867–870 (2000).
25. R. Hofferbert, H. Alt, C. Dembowski, H.-D. Gräf, H. L. Harney, A. Heine, H. Rehfeld, A. Richter, Experimental investigations of chaos-assisted tunneling in a microwave annular billiard. *Phys. Rev. E* **71**, 046201 (2005).
26. B. Dietz, T. Guhr, B. Gutkin, M. Miski-Oglu, A. Richter, Spectral properties and dynamical tunneling in constant-width billiards. *Phys. Rev. E* **90**, 022903 (2014).

27. S. Shinohara, T. Harayama, T. Fukushima, M. Hentschel, T. Sasaki, E. E. Narimanov, Chaos-assisted directional light emission from microcavity lasers. *Phys. Rev. Lett.* **104**, 163902 (2010).
28. E. Ott, *Chaos in Dynamical Systems* (Cambridge Univ. Press, 2002).
29. J. Laskar, The chaotic motion of the solar system: A numerical estimate of the size of the chaotic zones. *Icarus* **88**, 266–291 (1990).
30. V. Petrov, V. Gáspár, J. Masere, K. Showalter, Controlling chaos in the Belousov—Zhabotinsky reaction. *Nature* **361**, 240–243 (1993).
31. A. L. Goldberger, D. R. Rigney, B. J. West, Chaos and fractals in human physiology. *Sci. Am.* **262**, 42–49 (1990).
32. C.-S. Poon, C. K. Merrill, Decrease of cardiac chaos in congestive heart failure. *Nature* **389**, 492–495 (1997).
33. M. E. Gilpin, Spiral chaos in a predator-prey model. *Am. Nat.* **113**, 306–308 (1979).
34. S. Rinaldi, S. Muratori, Y. Kuznetsov, Multiple attractors, catastrophes and chaos in seasonally perturbed predator-prey communities. *Bull. Math. Biol.* **55**, 15–35 (1993).
35. E. Ott, C. Grebogi, J. A. Yorke, Controlling chaos. *Phys. Rev. Lett.* **64**, 1196–1199 (1990).
36. S. Boccaletti, C. Grebogi, Y.-C. Lai, H. Mancini, D. Maza, The control of chaos: Theory and applications. *Phys. Rep.* **329**, 103–197 (2000).
37. A. L. Fradkov, R. J. Evans, B. R. Andrievsky, Control of chaos: Methods and applications in mechanics. *Phil. Trans. R. Soc. A* **364**, 2279–2307 (2006).
38. B. V. Chirikov, A universal instability of many-dimensional oscillator systems. *Phys. Rep.* **52**, 263–379 (1979).
39. G. Casati, B. Chirikov, *Quantum Chaos: Between Order and Disorder* (Cambridge Univ. Press, 2006).
40. A. Mouchet, C. Miniatura, R. Kaiser, B. Grémaud, D. Delande, Chaos-assisted tunneling with cold atoms. *Phys. Rev. E* **64**, 016221 (2001).
41. R. Dubertrand, J. Billy, D. Guéry-Odelin, B. Georgeot, G. Lemarié, Routes towards the experimental observation of the large fluctuations due to chaos-assisted tunneling effects with cold atoms. *Phys. Rev. A* **94**, 043621 (2016).
42. M. V. Berry, M. Robnik, Semiclassical level spacings when regular and chaotic orbits coexist. *J. Phys. A* **17**, 2413–2421 (1984).
43. O. Bohigas, S. Tomsovic, D. Ullmo, Manifestations of classical phase space structures in quantum mechanics. *Phys. Rep.* **223**, 43–133 (1993).
44. M. J. Davis, E. J. Heller, Quantum dynamical tunneling in bound states. *J. Chem. Phys.* **75**, 246–254 (1981).
45. S. Keshavamurthy, P. Schlagheck, *Dynamical Tunneling: Theory and Experiment* (CRC Press, 2011).
46. F. Leyvraz, D. Ullmo, The level splitting distribution in chaos-assisted tunnelling. *J. Phys. A* **29**, 2529–2551 (1996).
47. O. Bohigas, D. Boosé, R. E. de Carvalho, V. Marvulle, Quantum tunneling and chaotic dynamics. *Nucl. Phys. A* **560**, 197–210 (1993).
48. S. Tomsovic, Chaos-assisted tunnelling in the absence of reflexion symmetry. *J. Phys. A Math. Gen.* **31**, 9469–9481 (1998).
49. S. C. Creagh, N. D. Whelan, Statistics of chaotic tunneling. *Phys. Rev. Lett.* **84**, 4084–4087 (2000).
50. A. D. Chepelianskii, D. L. Shepelyansky, Simulation of chaos-assisted tunneling in a semiclassical regime on existing quantum computers. *Phys. Rev. A* **66**, 054301 (2002).
51. A. Bäcker, R. Ketzmerick, S. Löck, Direct regular-to-chaotic tunneling rates using the fictitious-integrable-system approach. *Phys. Rev. E* **82**, 056208 (2010).
52. T. Onishi, A. Shudo, K. S. Ikeda, K. Takahashi, Tunneling mechanism due to chaos in a complex phase space. *Phys. Rev. E* **64**, 025201 (2001).
53. V. A. Podolskiy, E. E. Narimanov, Semiclassical description of chaos-assisted tunneling. *Phys. Rev. Lett.* **91**, 263601 (2003).
54. O. Brodier, P. Schlagheck, D. Ullmo, Resonance-assisted tunneling in near-integrable systems. *Phys. Rev. Lett.* **87**, 064101 (2001).
55. O. Brodier, P. Schlagheck, D. Ullmo, Resonance-assisted tunneling. *Ann. Phys.* **300**, 88–136 (2002).
56. A. Mouchet, C. Eltschka, P. Schlagheck, Influence of classical resonances on chaotic tunneling. *Phys. Rev. E* **74**, 026211 (2006).
57. C. Eltschka, P. Schlagheck, Resonance- and chaos-assisted tunneling in mixed regular-chaotic systems. *Phys. Rev. Lett.* **94**, 014101 (2005).
58. A. Ishikawa, A. Tanaka, A. Shudo, Quantum suppression of chaotic tunnelling. *J. Phys. A* **40**, F397–F405 (2007).
59. A. Shudo, Y. Ishii, K. S. Ikeda, Chaos attracts tunneling trajectories: A universal mechanism of chaotic tunneling. *Europhys. Lett.* **81**, 50003 (2008).
60. A. Bäcker, R. Ketzmerick, S. Löck, L. Schilling, Regular-to-chaotic tunneling rates using a fictitious integrable system. *Phys. Rev. Lett.* **100**, 104101 (2008).
61. N. Mertig, S. Löck, A. Bäcker, R. Ketzmerick, A. Shudo, Complex paths for regular-to-chaotic tunnelling rates. *Europhys. Lett.* **102**, 10005 (2013).
62. S. Löck, A. Bäcker, R. Ketzmerick, P. Schlagheck, Regular-to-chaotic tunneling rates: From the quantum to the semiclassical regime. *Phys. Rev. Lett.* **104**, 114101 (2010).
63. E. V. H. Doggen, B. Georgeot, G. Lemarié, Chaos-assisted tunneling in the presence of anderson localization. *Phys. Rev. E* **96**, 040201 (2017).
64. A. Bäcker, R. Ketzmerick, S. Löck, M. Robnik, G. Vidmar, R. Höhmann, U. Kuhl, H.-J. Stöckmann, Dynamical tunneling in mushroom billiards. *Phys. Rev. Lett.* **100**, 174103 (2008).
65. M.-W. Kim, S. Rim, C.-H. Yi, C.-M. Kim, Chaos-assisted tunneling in a deformed microcavity laser. *Opt. Express* **21**, 32508–32515 (2013).
66. W. K. Hensinger, H. Häffner, A. Browaeys, N. R. Heckenberg, K. Helmerson, C. McKenzie, G. J. Milburn, W. D. Phillips, S. L. Rolston, H. Rubinsztein-Dunlop, B. Upcroft, Dynamical tunnelling of ultracold atoms. *Nature* **412**, 52–55 (2001).
67. V. Averbukh, S. Osovski, N. Moiseyev, Controlled tunneling of cold atoms: From full suppression to strong enhancement. *Phys. Rev. Lett.* **89**, 253201 (2002).
68. A. Mouchet, D. Delande, Signatures of chaotic tunneling. *Phys. Rev. E* **67**, 046216 (2003).
69. I. Kovacic, R. Rand, S. Mohamed Sah, Mathieu's equation and its generalizations: Overview of stability charts and their features. *Appl. Mech. Rev.* **70**, 020802 (2018).
70. W. K. Hensinger, A. Mouchet, P. S. Julienne, D. Delande, N. R. Heckenberg, H. Rubinsztein-Dunlop, Analysis of dynamical tunneling experiments with a bose-einstein condensate. *Phys. Rev. A* **70**, 013408 (2004).
71. A. Fortun, C. Cabrera-Gutiérrez, G. Condon, E. Michon, J. Billy, D. Guéry-Odelin, Direct tunneling delay time measurement in an optical lattice. *Phys. Rev. Lett.* **117**, 010401 (2016).
72. C. Cabrera-Gutiérrez, E. Michon, M. Arnal, G. Chatelain, V. Brunaud, T. Kawalec, J. Billy, D. Guéry-Odelin, Resonant excitations of a bose einstein condensate in an optical lattice. *Eur. Phys. J. D* **73**, 170 (2019).
73. C. Cabrera-Gutiérrez, E. Michon, V. Brunaud, T. Kawalec, A. Fortun, M. Arnal, J. Billy, D. Guéry-Odelin, Robust calibration of an optical-lattice depth based on a phase shift. *Phys. Rev. A* **97**, 043617 (2018).
74. W. K. Hensinger, B. Upcroft, C. A. Holmes, N. R. Heckenberg, G. J. Milburn, H. Rubinsztein-Dunlop, Multiple bifurcations in atom optics. *Phys. Rev. A* **64**, 063408 (2001).
75. P. Leboeuf, A. Mouchet, Normal forms and complex periodic orbits in semiclassical expansions of hamiltonian systems. *Ann. Phys.* **275**, 54–112 (1999).
76. J. Tomkovič, W. Muessel, H. Strobel, S. Löck, P. Schlagheck, R. Ketzmerick, M. K. Oberthaler, Experimental observation of the poincaré-birkhoff scenario in a driven many-body quantum system. *Phys. Rev. A* **95**, 011602 (2017).
77. S. Inouye, M. Andrews, J. Stenger, H.-J. Miesner, D. Stamper-Kurn, W. Ketterle, Observation of Feshbach resonances in a Bose–Einstein condensate. *Nature* **392**, 151–154 (1998).
78. S. Fölling, S. Trotzky, P. Cheinet, M. Feld, R. Saers, A. Widera, T. Müller, I. Bloch, Direct observation of second-order atom tunnelling. *Nature* **448**, 1029–1032 (2007).
79. Y.-A. Chen, S. Nascimbène, M. Aidelsburger, M. Atala, S. Trotzky, I. Bloch, Controlling correlated tunneling and superexchange interactions with ac-driven optical lattices. *Phys. Rev. Lett.* **107**, 210405 (2011).
80. F. Meinert, M. J. Mark, E. Kirilov, K. Lauber, P. Weinmann, M. Gröbner, A. J. Daley, H.-C. Nägerl, Observation of many-body dynamics in long-range tunneling after a quantum quench. *Science* **344**, 1259–1262 (2014).
81. F. Evers, A. D. Mirlin, Anderson transitions. *Rev. Mod. Phys.* **80**, 1355–1417 (2008).
82. D. Sherrington, S. Kirkpatrick, Solvable model of a spin-glass. *Phys. Rev. Lett.* **35**, 1792–1796 (1975).
83. E. Khatami, A. Macridin, M. Jarrell, Effect of long-range hopping on T_c in a two-dimensional Hubbard-Holstein model of the cuprates. *Phys. Rev. B* **78**, 060502 (2008).
84. S.-J. Chang, K.-J. Shi, Evolution and exact eigenstates of a resonant quantum system. *Phys. Rev. A* **34**, 7–22 (1986).

Acknowledgments: We thank M. Burgher for experimental support. We thank P. Schlagheck and B. Peaudecerf for useful discussions. Computational resources were provided by the facilities of Calcul en Midi-Pyrénées (CALMIP). **Funding:** This work was supported by Programme Investissements d'Avenir under the program ANR-11-IDEX-0002-02, reference ANR-10-LABX-0037-NEXT, and research funding grant no. ANR-17-CE30-0024. M.A. acknowledges support from the DGA (Direction Générale de l'Armement), and N.D. acknowledges support from Région Occitanie and the Université Paul Sabatier. **Author contributions:** M.A., G.C., N.D., J.B., and D.G.-O. conducted the experiments. M.M., B.G., and G.L. performed the theoretical analysis. All authors edited and reviewed the manuscript. O.G., D.U., B.G., G.L., J.B., and D.G.-O. supervised the work. **Competing interests:** The authors declare that they have no competing interests. **Data and materials availability:** All data needed to evaluate the conclusions in the paper are present in the paper and/or the Supplementary Materials. Additional data related to this paper may be requested from the authors.

Submitted 27 April 2020
Accepted 29 July 2020
Published 18 September 2020
10.1126/sciadv.abc4886

Citation: M. Arnal, G. Chatelain, M. Martinez, N. Dupont, O. Giraud, D. Ullmo, B. Georgeot, G. Lemarié, J. Billy, D. Guéry-Odelin, Chaos-assisted tunneling resonances in a synthetic Floquet superlattice. *Sci. Adv.* **6**, eabc4886 (2020).

Chaos-assisted tunneling resonances in a synthetic Floquet superlattice

M. Arnal, G. Chatelain, M. Martinez, N. Dupont, O. Giraud, D. Ullmo, B. Georgeot, G. Lemarié, J. Billy and D. Guéry-Odelin

Sci Adv **6** (38), eabc4886.
DOI: 10.1126/sciadv.abc4886